frontiers in Chemical Engineering

ORIGINAL RESEARCH
published: 02 February 2022
doi: 10.3389/fceng.2022.828054

Solid Electrolyte Interphase Growth in Lithium Metal Cells With Normal Electrolyte Flow

Mihir N. Parekh[1]* *and Christopher D. Rahn*[2]

[1]*Department of Chemistry and Biochemistry, University of South Carolina, Columbia, SC, United States,* [2]*Department of Mechanical Engineering, Pennsylvania State University, University Park, PA, United States*

In high energy density lithium metal batteries (LMBs), dendrite and solid electrolyte interphase (SEI) growth reduce safety and longevity, respectively. A stable SEI layer enables high efficiency cycling but continued SEI growth can lead to reduced capacity and coulombic efficiency. In this paper, we develop a steady-state model that predicts the effect of small advective electrolyte flow towards the lithium metal electrode on SEI growth during charging. For a fixed current density, increasing the electrolyte flow rate improves the coulombic efficiency and decreases SEI layer growth rate. Decreasing the charging current density at a constant flow rate also decreases the SEI layer growth rate. Low flow rates ($\mu m/s$) can increase coulombic efficiency by up to 6%. The sensitivity of the coulombic efficiency to plating and SEI layer reaction rates is also explored.

Keywords: solid electrolyte interphase, lithium metal cells, normal electrolyte flow, coulombic efficiency, dendrite

OPEN ACCESS

Edited by:
Mingheng Li,
California State Polytechnic University, Pomona, United States

Reviewed by:
Hiroki Habazaki,
Hokkaido University, Japan
Ian Johnson,
Argonne National Laboratory (DOE), United States

****Correspondence:***
Mihir N Parekh
mp70@mailbox.sc.edu

Specialty section:
This article was submitted to Computational Methods in Chemical Engineering, a section of the journal Frontiers in Chemical Engineering

Received: *02 December 2021*
Accepted: *13 January 2022*
Published: *02 February 2022*

Citation:
Parekh MN and Rahn CD (2022) Solid Electrolyte Interphase Growth in Lithium Metal Cells With Normal Electrolyte Flow. Front. Chem. Eng. 4:828054. doi: 10.3389/fceng.2022.828054

1 INTRODUCTION

Lithium metal batteries are promising, energy-dense next generation batteries (Whittingham, 2012). Electroplating during charging, however can lead to dendrite growth on the metal electrodes. Moreover, due to their high reactivity, metal electrodes often react instantaneously with the electrolyte to form a solid electrolyte interphase (SEI) (Peled, 1979). Stripping Li from under the SEI during discharging can lead to the formation of nanovoids. Aggregation of nanovoids at high discharge rates can lead to the collapse of the SEI layer (pitting), exposing fresh Li surfaces and consuming further Li (Shi et al., 2018) in SEI generation. These inhomogeneities in the Li metal surface formed due to repeated stripping and pitting produce surface irregularities that promote dendrite growth. Discharging at high current can lead to rapid SEI growth and increased impedance, thus making fast charging difficult. This mechanism is the root cause of failure in Li metal batteries (Lu et al., 2015). Cracking of the SEI around dendrite tips due to excessive stress also promotes dendrite growth (Liu and Lu, 2017). A mechanically tough SEI may withstand stress, reduce dendrite growth, and prevent consumption of Li during repeated cycling as fresh Li surfaces are not exposed to the electrolyte if the SEI layer does not break (Aurbach, 2000). SEI layer growth has been studied extensively in theoretical, computational, first-principles modeling, and experimental studies (Jiang et al., 2020).

Modeling plays a key role in understanding the SEI growth mechanism. The model based on electron-tunneling proposed by Peled (1979) is one of the pioneering works in this field. Broussely et al. (2001) propose a growth model limited by electronic conductivity of the SEI layer and link SEI layer growth to capacity degradation and aging in Li ion batteries. Ploehn et al. (2004) propose a growth mechanism dominated by solvent diffusion through the SEI layer. Christensen and Newman (2004) derive a mathematical model for SEI layer growth and investigate the dependence of SEI layer

growth on battery voltage. They argue that the characteristics and chemical composition of SEI layers on lithium and graphite electrodes are similar. Pinson and Bazant (2012) derive the square root dependence of long term SEI layer growth on time using single particle and porous electrode models and a solvent diffusion limited growth mechanism. Their models fit the experimental data obtained by Broussely et al. (2001), Smith et al. (2011). The long term square root dependence may also be derived by using growth mechanisms associated with electronic conduction or neutral lithium interstitial diffusion through the SEI layer Single et al., 2018. A linear dependence of SEI growth with time results from linearization of the single particle model and SEI growth rate kinetics (Tanim and Rahn, 2015). Single et al. (2018) show that a growth mechanism limited by diffusion of lithium interstitials through the SEI can reproduce the potential dependence of long term SEI growth. With increasing SEI porosity, the SEI growth mechanism transitions from electronic conduction limited growth to solvent diffusion limited growth. Attia et al. (2019) experimentally show that even within the same charge-discharge cycle the SEI layer growth is faster while charging than during discharging. Das et al. (2019) build a theoretical model based on a mixed ionic electronic conductor SEI to explain these experimental results. The SEI may act as an electronic conductor, an ionic conductor, or a mixed electronic-ionic conductor or allow lithium interstitials to diffuse through or allows all of these phenomena. The mechanistic origin of the limiting mechanism of SEI growth is unclear.

Experimentally SEI evolution has mostly been studied via electrochemical impedance spectroscopy (Lu et al., 2014). Researchers have also studied SEI chemistry using various techniques such as XPS and FT-IR (Verma et al., 2010; Fan et al., 2018a). It is difficult to determine the SEI composition because it contains many compounds and functional groups. The composition also depends on the surface finish, electrolyte, cycling rates, temperatures, *etc.*, complicating experimental assessment of the SEI (Single et al., 2017). Calendar aging of lithium batteries occurs due to the chemical SEI formation and the effect of temperature and SOC on calendar aging has been studied experimentally by Keil et al. (2016), Keil and Jossen (2016). SEI also grows electrochemically during cell cycling. Factors such as potential, cycle number, and charging/discharging rate have been experimentally shown to govern the electrochemical SEI formation. Even at the same voltage, SEI formation rate is greater for the charging half cycle than for the discharging half cycle Attia et al., 2019.

Kim et al. (2011) study the effect of electrolyte composition on structure and evolution of SEI via molecular dynamics simulations. Bertolini and Balbuena (2018) use reactive molecular dynamics simulations to study the initial stages of formation of SEI on Li metal electrodes in the absence of a bias potential. They identify a porous phase in contact with the Li metal electrode, a nest phase (amorphous matrix of Li atoms separated by nanochannels which allow electrolyte molecules and decomposition products to diffuse through), and a disperse phase in the SEI (layer in contact with the electrolyte) and propose that uneven Li distribution in the nest and dispersed phases may be responsible for uneven electric field and dendrite growth.

The SEI layer often contains both organic and inorganic products (Aurbach, 2000; Michan et al., 2016) and its composition depends upon electrolyte composition (Matsuda, 1993; Aurbach and Zaban, 1993), temperature (Ishikawa et al., 2001) and charge-discharge current (Dolle et al., 2001). A stable SEI is thought to prevent dendrite growth, so researchers use SEI forming additives such as vinylene carbonate (Ota et al., 2004; Aurbach et al., 2002; El Ouatani et al., 2008) triacetoxyvinylsilane (Lee et al., 2007), fluoroethylene carbonate (Heine et al., 2015), organosulphides (Li et al., 2017), aluminium fluoride (for cathode electrolyte interphase) (Zhao et al., 2020) in the electrolyte and grow artificial SEI layers *in-situ* (Li et al., 2016; Pathak et al., 2020) and *ex-situ* (Wang et al., 2019; Gao et al., 2019; Ju et al., 2020). Indirect strategies to stabilize the SEI include changing electrolyte concentration (Fan X. et al., 2018; Wang et al., 2018) and modifying the host (Cui et al., 2020; Liu et al., 2020) and separator (Huo et al., 2020; Liang et al., 2020) materials. Reported coulombic efficiencies range from 92% (Ma et al., 2017) to 99.1% (Gao et al., 2019).

The emerging area of flowing electrolyte metal batteries (FEMBs) has demonstrated dendrite suppression both theoretically (Parekh et al., 2020; Parekh and Rahn, 2020a; Parekh and Rahn, 2020b) and experimentally (Huang et al., 2020). In Parekh et al. (2020), Parekh M. and Rahn C. (2020), creeping flow normal to the lithium metal electrode and above a critical speed can theoretically eliminate dendrite growth. Creeping flow parallel to the lithium metal electrode can also reduce dendrite growth (Parekh M. N. and Rahn C. D., 2020). Dendrite and SEI layer growth in LMBs are inherently coupled. Our earlier efforts (Parekh et al., 2020; Parekh M. N. and Rahn C. D., 2020; Parekh M. and Rahn C., 2020) focused on effects of advection on dendrite growth and neglected SEI growth. This paper develops the first steady-state model of a lithium metal electrode with normal electrolyte flow that includes solvent diffusion and SEI layer growth kinetics. The model predicts the current distribution between plating and SEI layer growth and also identifies the reaction parameters that may be required to achieve high coulombic efficiencies. To the best of authors' knowledge, there has been no previous experimental study on the effect of electrolyte flow on SEI growth and the authors intend to explore that in the future.

2 GOVERNING EQUATIONS

Figure 1 shows a schematic diagram of the Li metal cell with electrolyte flow normal to the lithium metal electrode. We assume that a charging current density J_{tot} leads to a flux $\mathbf{N_c}$ which transports Li^+ ions from the positive electrode at $Z = 0$ to the Li metal electrode at $Z = L$ where they may either plate or be consumed to generate SEI. We also assume the electrodes to be perforated or porous (*e.g.,* metal foam) with sufficiently fine scaled pore structure to allow uniform normal electrolyte flow. The SEI layer on the porous electrodes is also assumed to be porous and much thinner than the inter-electrode gap. This

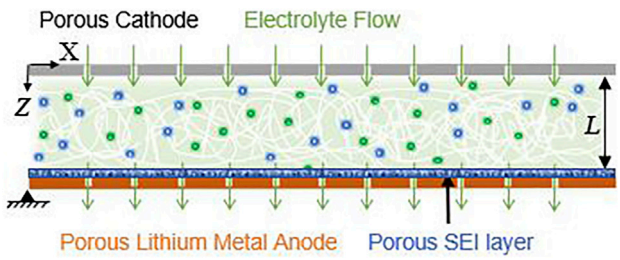

FIGURE 1 | Schematic diagram of the lithium metal cell model with uniform normal electrolyte flow through porous Solid Electrolyte Interphase (SEI) layer and porous electrodes.

means that we do not account for the temporal evolution of SEI thickness and also do not account for self passivating behavior of the SEI (*i.e.,* neglect solvent, ion and lithium interstitial diffusion and electronic conduction through SEI). With a flowing electrolyte and a porous SEI, advective transport in the bulk electrolyte is assumed to be the dominant mechanism governing SEI growth.

Within the electrolyte (neglecting the double layer region)

$$0 = -\nabla \cdot \mathbf{N_c}, \tag{1}$$

$$0 = D_c \frac{\partial^2 C_c}{\partial Z^2} + \mu_c F C_c \frac{\partial^2 \Phi}{\partial Z^2} + \mu_c F \frac{\partial C_c}{\partial Z}\frac{\partial \Phi}{\partial Z} - v\frac{\partial C_c}{\partial Z}, \tag{2}$$

$$0 = D_a \frac{\partial^2 C_a}{\partial Z^2} - \mu_a F C_a \frac{\partial^2 \Phi}{\partial Z^2} - \mu_a F \frac{\partial C_a}{\partial Z}\frac{\partial \Phi}{\partial Z} - v\frac{\partial C_a}{\partial Z}, \tag{3}$$

where F is Faraday's constant, D is diffusivity, μ is electric mobility, $\mathbf{N_c}$ is the solute flux, $C(Z)$ is solute (ion) concentration, $\mathbf{v} = v\hat{\mathbf{k}}$ is the electrolyte velocity, and $\Phi(Z)$ is electrostatic potential. The subscripts c and a indicate cation and anion respectively. Electroneutrality requires

$$C_c = C_a = C. \tag{4}$$

Using **Eqs 2–4** gives

$$0 = D\frac{\partial^2 C}{\partial Z^2} - v\frac{\partial C}{\partial Z}, \tag{5}$$

where $D = \frac{2D_cD_a}{D_c+D_a}$ is the ambipolar diffusivity. Comparing **Eqs 1, 5** gives

$$\mathbf{N_c} = \left(-D\frac{\partial C}{\partial Z} + vC\right)\hat{\mathbf{k}}. \tag{6}$$

Solvent transport is governed by

$$0 = -\nabla \cdot \mathbf{N_s}, \tag{7}$$

$$\mathbf{N_s} = \left(-D_s\frac{\partial C_s}{\partial Z} + vC_s\right)\hat{\mathbf{k}} \tag{8}$$

where $\mathbf{N_s}$ is the solvent flux, C_s is the concentration of the solvent, and D_s is the solvent diffusivity. The total charging current density is divided between plating current density J_p and SEI formation current density J_{sei}, so

$$J_{tot} = J_{sei} + J_p, \tag{9}$$

where the current densities are given by the Butler-Volmer equations

$$J_p = F\mathbf{N_c}(L)\cdot\hat{\mathbf{k}} \tag{10}$$

$$J_p = K_pC_c(L,T)^{1-\alpha}\left[exp\left(\frac{-\alpha FN_p}{RT_0}\right) - exp\left(\frac{\alpha FN_p}{RT_0}\right)\right] \tag{11}$$

and

$$J_{sei} = F\mathbf{N_s}(L)\cdot\hat{\mathbf{k}} \tag{12}$$

$$J_{sei} = K_{sei}[C_c(L)C_s(L)]^{1-\alpha}\left[exp\left(\frac{-\alpha FN_{sei}}{RT_0}\right) - exp\left(\frac{\alpha FN_{sei}}{RT_0}\right)\right] \tag{13}$$

where N_p and N_{sei} are the activation overpotentials for plating and SEI formation, K_p and K_{sei} are the pre-exponential factors for plating and SEI formation, respectively, α is the symmetry factor, and T_0 is the temperature.

Non dimensional variables are defined as, $j_{tot} = \frac{J_{tot}L}{FD_cC_0}$, $d = \frac{D}{D_c}$, $d_s = \frac{D_s}{D_c}$, $Pe = \frac{vL}{D_c}$, $\phi = \frac{\Phi F}{RT_0}$, $c_c = \frac{C_c}{C_0}$, $c_a = \frac{C_a}{C_0}$, $c_s = \frac{C_s}{C_0}$, $z = \frac{Z}{L}$, $\mathbf{n_c} = \frac{\mathbf{N_c}L}{D_cC_0}$, $\mathbf{n_s} = \frac{\mathbf{N_s}L}{D_cC_0}$ $j_{sei} = \frac{J_{sei}L}{FD_cC_0}$, $j_p = \frac{J_pL}{FD_cC_0}$, $\eta_p = \frac{FN_p}{RT_0}$, $\eta_{sei} = \frac{FN_{sei}}{RT_0}$, $k_p = \frac{K_pL}{FD_cC_0^{0.5}}$, and $k_{sei} = \frac{K_{sei}L}{FD_c}$ where C_0 and C_{0s} are the average solute and solvent concentrations, respectively. Substituting these variables in **Eqs 5–13** produces

$$0 = \frac{\partial^2 c_c}{\partial z^2} + c_c\frac{\partial^2 \phi}{\partial z^2} + \frac{\partial c_c}{\partial z}\frac{\partial \phi}{\partial z} - Pe\frac{\partial c_c}{\partial z} \tag{14}$$

$$0 = \frac{\partial^2 c_a}{\partial z^2} - c_a\frac{\partial^2 \phi}{\partial z^2} - \frac{\partial c_a}{\partial z}\frac{\partial \phi}{\partial z} - Pe\frac{D_c}{D_a}\frac{\partial c_a}{\partial z} \tag{15}$$

$$c_c = c_a = c, \tag{16}$$

$$0 = d\frac{\partial^2 c}{\partial z^2} - Pe\frac{\partial c}{\partial z}, \tag{17}$$

$$\mathbf{n_c} = \left(-d\frac{\partial c}{\partial z} + Pec\right)\hat{\mathbf{k}}, \tag{18}$$

$$0 = d_s\frac{\partial^2 c_s}{\partial z^2} - Pe\frac{\partial c}{\partial z}, \tag{19}$$

$$\mathbf{n_s} = \left(-d_s\frac{\partial c_s}{\partial z} + Pec_s\right)\hat{\mathbf{k}}, \tag{20}$$

$$j_{tot} = j_p + j_{sei}, \tag{21}$$

$$j_p = k_pc_c(1)^{1-\alpha}\left[exp\left(-\alpha\eta_p\right) - exp\left((1-\alpha)\eta_p\right)\right], \tag{22}$$

$$j_{sei} = k_{sei}c_c(1)^{1-\alpha}c_s(1)^{1-\alpha}\left[exp\left(-\alpha\eta_{sei}\right) - exp\left((1-\alpha)\eta_{sei}\right)\right]. \tag{23}$$

The equilibrium potential for SEI formation is assumed to be 0.8 V (Harris and Lu, 2013). Also, the plating and SEI formation reactions are assumed to be happening parallelly. So,

$$\frac{RT_0}{F}ln(C_c(L)) + N_p = 0.8 + N_{sei}. \tag{24}$$

Non-dimensionalizing **Eq. 24** gives

$$\eta_p + ln(c(1)) + 6.909 = \eta_{sei} + 0.8F\big/(RT_0). \tag{25}$$

The nondimensional model given by **Eqs 14–25** differs from those in previous work (Parekh et al., 2020; Parekh M. and Rahn

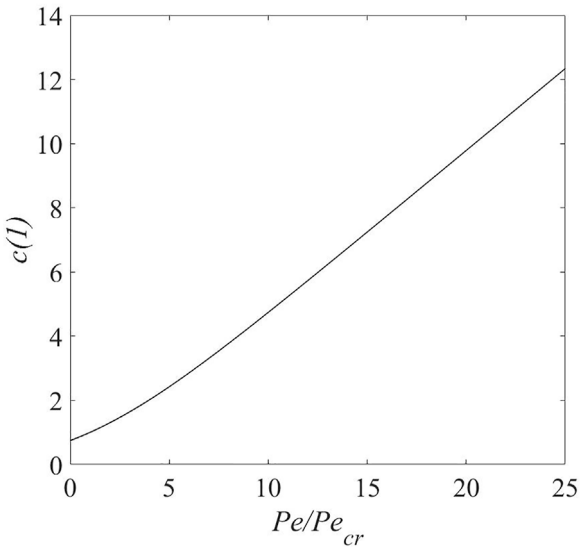

FIGURE 2 | Electrolyte concentration at lithium metal electrode-electrolyte interface versus flow rate for $j = 1$.

C., 2020; Parekh M. N. and Rahn C. D., 2020) in two important ways. The solvent transport (**Eq. 19**) and the SEI layer kinetics (**Eq. 23**) have been added.

We use **Eqs 18**, **20** as boundary conditions at both $z = 0$ and $z = 1$. Using these boundary conditions, **Eqs 17**, **19**, **21**–**23** and **25** are solved analytically to produce

$$c = \frac{j_{tot}}{Pe} + \left[c_{a0} - \frac{j_{tot}}{Pe}\right] \exp\left(zPe/d\right), \tag{26}$$

$$c_{a0} = \frac{j_{tot}}{Pe} + \frac{\left[1 - \frac{j_{tot}}{Pe}\right]\left[Pe/d\right]}{\exp\left(Pe/d\right) - 1}, \tag{27}$$

$$c_s = \frac{j_{sei}}{Pe} + \left[c_{sa0} - \frac{j_{sei}}{Pe}\right] \exp\left(zPe/d_s\right), \tag{28}$$

$$c_{sa0} = \frac{j_{sei}}{Pe} + \frac{\left[1 - \frac{j_{sei}}{Pe}\right]\left[Pe/d_s\right]}{\exp\left(Pe/d_s\right) - 1}. \tag{29}$$

3 RESULTS

The critical Peclet number, Pe_{cr}, is defined as the Peclet number at which advective flux equals the total ionic flux at the negative electrode. Our previous analysis (Parekh et al., 2020) shows that at steady state, critical flow rate or $Pe = Pe_{cr}$ leads to an almost uniform concentration profile given by $c = 1$ and hence we use that to calculate Pe_{cr}.

Based on our previous results (Parekh et al., 2020), we expect the concentration gradient and electrostatic potential gradient to reduce in magnitude with increasing flow rate and then the gradients change sign above the critical flow rate. **Figure 2** shows that the electrolyte concentration at the lithium metal electrode surface increases with increasing flow rate. Based on **Eqs 26**–**29**, the solvent concentration is expected to follow a similar pattern. It is important to note this trend because concentration of both electrolyte and solvent is expected to have an effect on SEI kinetics as per **Eqs (22)**–**(25)**.

TABLE 1 | Model parameters.

Property	Value
C_0	1 M
C_{0s}	4.5 M Single et al. (2017)
T_0	300 K
L	50 μm
D_a	$4E - 10$ m^2s^{-1} Tikekar et al. (2014)
D_c	10^{-11} m^2s^{-1} (Akolkar (2014))
D_s	$10^{-10} - 10^{-8}$ m^2s^{-1}
F	96,500 $Cmol^{-1}$
R	8.314 $Jmol^{-1}K^{-1}$
μ_c	$D_c/(RT_0)$ $mols^{-1}N^{-1}$
μ_a	$D_a/(RT_0)$ $mols^{-1}N^{-1}$
α	0.5 Das et al. (2019)
K_p	$1.1E - 2$ $Am^{-2}mol^{-0.5}m^{1.5}$ Das et al. (2019)
K_{sei}	$2.5E - 9/C_{0s}^{0.5}$ $Am^{-2}mol^{-1}m^3$ Das et al. (2019)

Assuming SEI layer formation and dead Li are the only Li sinks other than plating, coulombic efficiency (CE) can be defined as

$$CE = \left(DC/CC\right) = \left(1 - DL/CC - SEIC/CC\right), \tag{30}$$

where DC is discharge capacity, CC is charge capacity, $SEIC$ is the charge capacity lost in SEI formation, and DL is the amount of dead Li. Flow rates above Pe_{cr} eliminate dendrites (Parekh et al., 2020). So we assume that dead Li is eliminated under these conditions, and

$$CE = \left(DC/CC\right) = \left(1 - SEIC/CC\right) = j_p \big/ j_{tot}. \tag{31}$$

Thus, increasing j_p/j_{tot} results in increased coulombic efficiency and cycle life. For typical charging current densities, Pe_{cr} is on the order of 1, so the dimensional critical velocity is on the order of D_c/L. For $j = 1$ and parameters in **Table 1**, the critical velocity is on the order of $\mu m\ s^{-1}$. Thus, the required flow rates are very low and may be practically achieved using a variety of low power microfluidic pumping systems (Iverson and Garimella, 2008) along with porous or micropatterned electrodes (Park et al., 2016; Ryou et al., 2015; Wang et al., 2017). Programmed squeezing of a battery pack composed of pouch cells is another way to achieve the desired electrolyte flow.

Figure 3 shows that increasing the flow rate increases the j_p/j_{tot} ratio. At $Pe = 15Pe_{cr}$, $d_s = 100$ and $j = 3$, coulombic efficiency of 99.3% is predicted. This is 6% higher than without electrolyte flow. **Figure 3** shows that at low flow rates (including $Pe = 0$), a high charging current density leads to a lower coulombic efficiency. This is similar to the experimental observations (Attia et al., 2019; Madani et al., 2019) and other models (Lu et al., 2015; Das et al., 2019) in literature. Most models (Ploehn et al., 2004; Pinson and Bazant, 2012; Das et al., 2019) in literature account for the SEI layer thickness evolution with time. We, however, assume the SEI layer thickness to be negligible with respect to the inter-electrode gap and hence do not account for the temporal evolution of its thickness. SEI layer thickness becomes important in cases where diffusion is the main ion

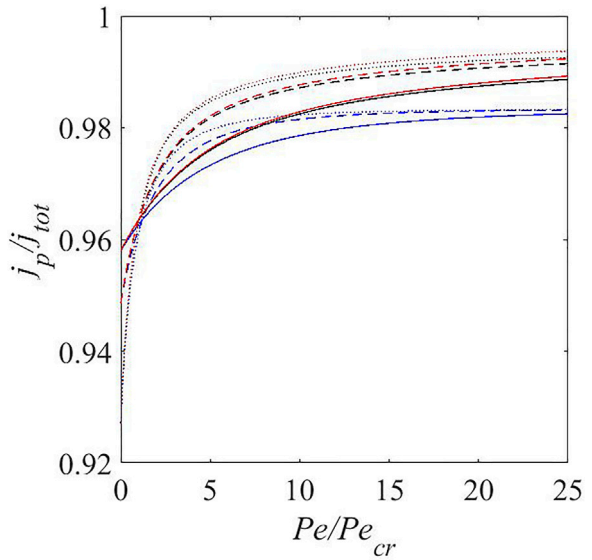

FIGURE 3 | Ratio of plating current to total current at steady state versus Pe/Pe_{cr} for j_{tot} = 1 (solid), j_{tot} = 2 (dashed), j_{tot} = 3 (dotted) at d_s = 10 (blue), d_s = 100 (black), and d_s = 1,000 (red).

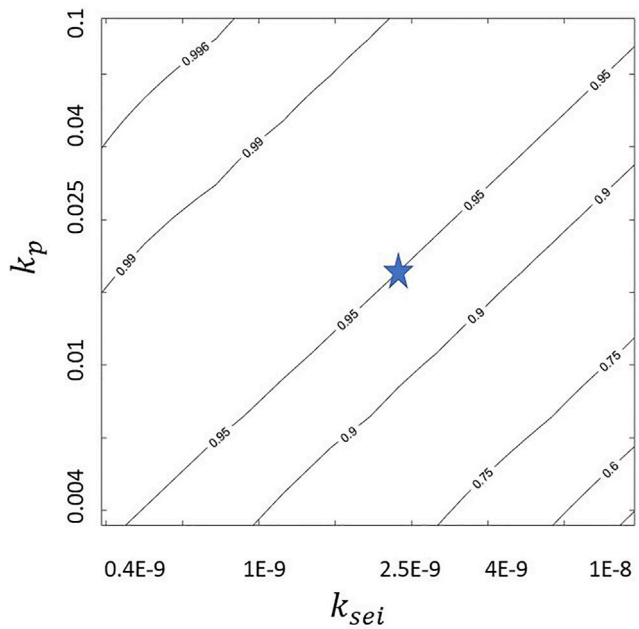

FIGURE 4 | Variation of j_p/j_{tot} at j_{tot} = 1, d_s = 100, and Pe = 0 with k_p and k_{sei} where "star" indicates values chosen for **Figure 3**.

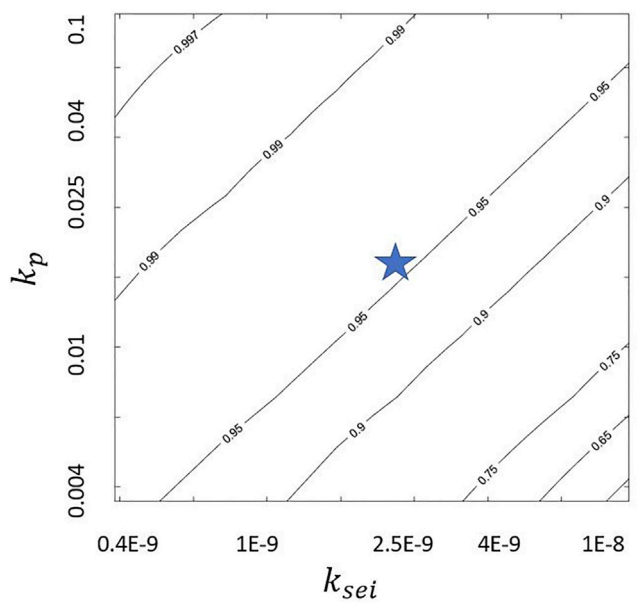

FIGURE 5 | Variation of j_p/j_{tot} at j_{tot} = 1, d_s = 100, and $Pe = Pe_{cr}$ with k_p and k_{sei} where "star" indicates values chosen for **Figure 3**.

transport mechanism as a thicker SEI layer acts as a self passivating layer by reducing ion and solvent diffusivity. However, for a flowing electrolyte, the main ion transport and solvent transport mechanism is assumed to be advective transport and we do not expect our results to get affected drastically by the SEI layer thickness. At higher flow rates, the coulombic efficiencies flatten with respect to increasing charging current density and increasing flow rates. Under these conditions, lithium ions concentrate near the lithium metal electrode and increasing flow rate leads to a marginal increase in lithium ions available near the lithium metal electrode. Current literature values for coulombic efficiency in lithium metal cells mostly lie between 92% (Ma et al., 2017)—99.1% (Gao et al., 2019). Electrolyte flow accelerates both solvent and ion advective transport, so one might expect equal effects on both. Solvent diffusivity, however, is typically much higher than ionic diffusivity. Thus, ionic transport benefits more from advective transport leading to an increased CE due to an increase in j_p and reduction in j_{sei}. The fact that increasing the flow rate increases the CE is valid for all the three different d_s values used in **Figure 3**. This indicates that the increase in CE with flow rates is not an artifact of the chosen solvent diffusivity.

The predicted CE values in **Figure 3** depends on the model parameters. We explore the sensitivity of CE to plating and SEI reaction constants. The nondimensional k_p = 0.018 and k_{sei} = $1.93E-9$ from literature (Das et al. (2019)) are varied by a factor of 5 in both directions. **Figures 4–6** show the variation of j_p/j_{tot} with k_p and k_{sei} values. They show that a higher k_p and a lower k_{sei} imply low SEI growth rate for galvanostatic charging. This is probably because higher k_p values and lower k_{sei} values imply higher and lower reaction rates for plating and SEI formation, respectively. This is also evident from **Eqs 21–23**. Moreover, a comparison of j_p/j_{tot} at same k_p and k_{sei} values indicates that a higher flow rate leads to higher coulombic efficiency. Finally, the top left corner of **Figure 6** shows coulombic efficiencies more than 99.9% for $k_p \approx 0.1$ and $k_{sei} \approx$ 0.4E-9 with higher k_p values requiring higher k_{sei} values for the same coulombic efficiency. This may enable practical applications with about 225 cycles

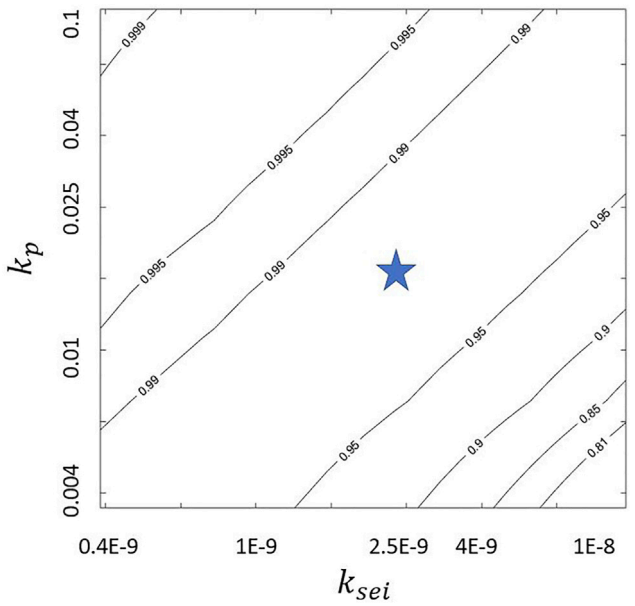

FIGURE 6 | Variation of j_p/j_{tot} at $j_{tot} = 1$, $d_s = 100$, and $Pe = 12.5Pe_{cr}$ with k_p and k_{sei} where "star" indicates values chosen for **Figure 3**.

(even when the self-passivating nature of SEI is excluded and excess lithium present in the lithium metal anode is not accounted for in the model). These figures may be used as a guideline to tune the flow rate and electrolyte/solvent (rate constants) so as to obtain practical lithium metal batteries. A comparison of **Figures 4**, **6** shows that just tuning the electrolyte parameters within the explored ranges will not allow us to reach the high coulombic efficiency of 99.9%. It is necessary to tune the electrolyte/solvent and also use normal electrolyte flow to achieve high coulombic efficiencies.

4 CONCLUSION

A small amount of electrolyte flow towards the metal electrode of a LMB during charging can produce remarkable results. As discussed in previous work (Parekh et al., 2020), electrostatic potential decreases and dendrites disappear, making LMBs amenable to fast charging and safe operation. This paper shows for the first time that flow reduces SEI layer formation and increases coulombic efficiency. The critical flow rate is a key parameter in the design of FEMBs. It is the lowest flow rate that suppresses dendrites. Tuning flow rates and electrolyte parameters such as rate constants can enable fast charging, safe, dendrite-free, long-lasting lithium metal batteries.

DATA AVAILABILITY STATEMENT

The original contributions presented in the study are included in the article/Supplementary Material, further inquiries can be directed to the corresponding author.

AUTHOR CONTRIBUTIONS

MNP is the first author and he built the model, generated the results, and wrote the manuscript. CDR is the last author and he guided MNP during the project, and edited the manuscript.

FUNDING

This research was partially supported by the National Science Foundation under Grant No. 1662055.

REFERENCES

Akolkar, R. (2014). Modeling Dendrite Growth during Lithium Electrodeposition at Sub-Ambient Temperature. *J. Power Sourc.* 246, 84–89. doi:10.1016/j.jpowsour.2013.07.056

Attia, P. M., Das, S., Harris, S. J., Bazant, M. Z., and Chueh, W. C. (2019). Electrochemical Kinetics of Sei Growth on Carbon Black: Part I. Experiments. *J. Electrochem. Soc.* 166, E97–E106. doi:10.1149/2.0231904jes

Aurbach, D., Gamolsky, K., Markovsky, B., Gofer, Y., Schmidt, M., and Heider, U. (2002). On the Use of Vinylene Carbonate (Vc) as an Additive to Electrolyte Solutions for Li-Ion Batteries. *Electrochimica acta* 47, 1423–1439. doi:10.1016/s0013-4686(01)00858-1

Aurbach, D. (2000). Review of Selected Electrode-Solution Interactions Which Determine the Performance of Li and Li Ion Batteries. *J. Power Sourc.* 89, 206–218. doi:10.1016/s0378-7753(00)00431-6

Aurbach, D., and Zaban, A. (1993). Impedance Spectroscopy of Lithium Electrodes. *J. Electroanalytical Chem.* 348, 155–179. doi:10.1016/0022-0728(93)80129-6

Bertolini, S., and Balbuena, P. B. (2018). Buildup of the Solid Electrolyte Interphase on Lithium-Metal Anodes: Reactive Molecular Dynamics Study. *J. Phys. Chem. C* 122, 10783–10791. doi:10.1021/acs.jpcc.8b03046

Broussely, M., Herreyre, S., Biensan, P., Kasztejna, P., Nechev, K., and Staniewicz, R. J. (2001). Aging Mechanism in Li Ion Cells and Calendar Life Predictions. *J. Power Sourc.* 97-98, 13–21. doi:10.1016/s0378-7753(01)00722-4

Christensen, J., and Newman, J. (2004). A Mathematical Model for the Lithium-Ion Negative Electrode Solid Electrolyte Interphase. *J. Electrochem. Soc.* 151, A1977. doi:10.1149/1.1804812

Cui, C., Yang, C., Eidson, N., Chen, J., Han, F., Chen, L., et al. (2020). A Highly Reversible, Dendrite-Free Lithium Metal Anode Enabled by a Lithium-Fluoride-Enriched Interphase. *Adv. Mater.* 32, 1906427. doi:10.1002/adma.201906427

Das, S., Attia, P. M., Chueh, W. C., and Bazant, M. Z. (2019). Electrochemical Kinetics of Sei Growth on Carbon Black: Part Ii. Modeling. *J. Electrochem. Soc.* 166, E107–E118. doi:10.1149/2.0241904jes

Dollé, M., Grugeon, S., Beaudoin, B., Dupont, L., and Tarascon, J.-M. (2001). *In Situ* tem Study of the Interface Carbon/Electrolyte. *J. Power Sourc.* 97-98, 104–106. doi:10.1016/s0378-7753(01)00507-9

El Ouatani, L., Dedryvère, R., Siret, C., Biensan, P., Reynaud, S., Iratçabal, P., et al. (2008). The Effect of Vinylene Carbonate Additive on Surface Film Formation on Both Electrodes in Li-Ion Batteries. *J. Electrochem. Soc.* 156, A103. doi:10.1149/1.3029674

Fan, L., Chen, S., Zhu, J., Ma, R., Li, S., Podila, R., et al. (2018a). Simultaneous Suppression of the Dendrite Formation and Shuttle Effect in a Lithium–Sulfur Battery by Bilateral Solid Electrolyte Interface. *Adv. Sci.* 5, 1700934. doi:10.1002/advs.201700934

Fan, X., Chen, L., Ji, X., Deng, T., Hou, S., Chen, J., et al. (2018b). Highly Fluorinated Interphases Enable High-Voltage Li-Metal Batteries. *Chem* 4, 174–185. doi:10.1016/j.chempr.2017.10.017

Gao, Y., Yan, Z., Gray, J. L., He, X., Wang, D., Chen, T., et al. (2019). Polymer–Inorganic Solid–Electrolyte Interphase for Stable Lithium Metal

Batteries under Lean Electrolyte Conditions. *Nat. Mater.* 18, 384–389. doi:10.1038/s41563-019-0305-8

Harris, S. J., and Lu, P. (2013). Effects of Inhomogeneities-Nanoscale to Mesoscale-On the Durability of Li-Ion Batteries. *J. Phys. Chem. C* 117, 6481–6492. doi:10.1021/jp311431z

Heine, J., Hilbig, P., Qi, X., Niehoff, P., Winter, M., and Bieker, P. (2015). Fluoroethylene Carbonate as Electrolyte Additive in Tetraethylene Glycol Dimethyl Ether Based Electrolytes for Application in Lithium Ion and Lithium Metal Batteries. *J. Electrochem. Soc.* 162, A1094–A1101. doi:10.1149/2.0011507jes

Huang, A., Liu, H., Manor, O., Liu, P., and Friend, J. (2020). Enabling Rapid Charging Lithium Metal Batteries via Surface Acoustic Wave-Driven Electrolyte Flow. *Adv. Mater.* 32, 1907516. doi:10.1002/adma.201907516

Huo, H., Li, X., Chen, Y., Liang, J., Deng, S., Gao, X., et al. (2020). Bifunctional Composite Separator with a Solid-State-Battery Strategy for Dendrite-free Lithium Metal Batteries. *Energ. Storage Mater.* 29, 361–366. doi:10.1016/j.ensm.2019.12.022

Ishikawa, M., Tasaka, Y., Yoshimoto, N., and Morita, M. (2001). Optimization of Physicochemical Characteristics of a Lithium Anode Interface for High-Efficiency Cycling: an Effect of Electrolyte Temperature. *J. Power Sourc.* 97-98, 262–264. doi:10.1016/s0378-7753(01)00621-8

Iverson, B. D., and Garimella, S. V. (2008). Recent Advances in Microscale Pumping Technologies: a Review and Evaluation. *Microfluid Nanofluid* 5, 145–174. doi:10.1007/s10404-008-0266-8

Jiang, Y., Wang, B., Liu, P., Wang, B., Zhou, Y., Wang, D., et al. (2020). Modified Solid-Electrolyte Interphase toward Stable Li Metal Anode. *Nano Energy* 77, 105308. doi:10.1016/j.nanoen.2020.105308

Ju, Z., Nai, J., Wang, Y., Liu, T., Zheng, J., Yuan, H., et al. (2020). Biomacromolecules Enabled Dendrite-Free Lithium Metal Battery and its Origin Revealed by Cryo-Electron Microscopy. *Nat. Commun.* 11, 1–10. doi:10.1038/s41467-020-14358-1

Keil, P., and Jossen, A. (2016). Calendar Aging of Nca Lithium-Ion Batteries Investigated by Differential Voltage Analysis and Coulomb Tracking. *J. Electrochem. Soc.* 164, A6066–A6074. doi:10.1149/2.0091701jes

Keil, P., Schuster, S. F., Wilhelm, J., Travi, J., Hauser, A., Karl, R. C., et al. (2016). Calendar Aging of Lithium-Ion Batteries. *J. Electrochem. Soc.* 163, A1872. doi:10.1149/2.0411609jes

Kim, S.-P., Duin, A. C. T. V., and Shenoy, V. B. (2011). Effect of Electrolytes on the Structure and Evolution of the Solid Electrolyte Interphase (Sei) in Li-Ion Batteries: A Molecular Dynamics Study. *J. Power Sourc.* 196, 8590–8597. doi:10.1016/j.jpowsour.2011.05.061

Lee, Y. M., Seo, J. E., Lee, Y.-G., Lee, S. H., Cho, K. Y., and Park, J.-K. (2007). Effects of Triacetoxyvinylsilane as Sei Layer Additive on Electrochemical Performance of Lithium Metal Secondary Battery. *Electrochem. Solid-State Lett.* 10, A216. doi:10.1149/1.2750439

Li, G., Gao, Y., He, X., Huang, Q., Chen, S., Kim, S. H., et al. (2017). Organosulfide-Plasticized Solid-Electrolyte Interphase Layer Enables Stable Lithium Metal Anodes for Long-Cycle Lithium-Sulfur Batteries. *Nat. Commun.* 8, 1–10. doi:10.1038/s41467-017-00974-x

Li, N.-W., Yin, Y.-X., Yang, C.-P., and Guo, Y.-G. (2016). An Artificial Solid Electrolyte Interphase Layer for Stable Lithium Metal Anodes. *Adv. Mater.* 28, 1853–1858. doi:10.1002/adma.201504526

Liang, J., Chen, Q., Liao, X., Yao, P., Zhu, B., Lv, G., et al. (2020). A Nano-Shield Design for Separators to Resist Dendrite Formation in Lithium-Metal Batteries. *Angew. Chem. Int. Edition* 59, 6561–6566. doi:10.1002/anie.201915440

Liu, G., and Lu, W. (2017). A Model of Concurrent Lithium Dendrite Growth, Sei Growth, Sei Penetration and Regrowth. *J. Electrochem. Soc.* 164, A1826–A1833. doi:10.1149/2.0381709jes

Liu, S., Ji, X., Yue, J., Hou, S., Wang, P., Cui, C., et al. (2020). High Interfacial-Energy Interphase Promoting Safe Lithium Metal Batteries. *J. Am. Chem. Soc.* 142, 2438–2447. doi:10.1021/jacs.9b11750

Lu, D., Shao, Y., Lozano, T., Bennett, W. D., Graff, G. L., Polzin, B., et al. (2015). Failure Mechanism for Fast-Charged Lithium Metal Batteries with Liquid Electrolytes. *Adv. Energ. Mater.* 5, 1400993. doi:10.1002/aenm.201400993

Lu, P., Li, C., Schneider, E. W., and Harris, S. J. (2014). Chemistry, Impedance, and Morphology Evolution in Solid Electrolyte Interphase Films during Formation in Lithium Ion Batteries. *J. Phys. Chem. C* 118, 896–903. doi:10.1021/jp4111019

Ma, L., Kim, M. S., and Archer, L. A. (2017). Stable Artificial Solid Electrolyte Interphases for Lithium Batteries. *Chem. Mater.* 29, 4181–4189. doi:10.1021/acs.chemmater.6b03687

Madani, S., Schaltz, E., and Knudsen Kær, S. (2019). Effect of Current Rate and Prior Cycling on the Coulombic Efficiency of a Lithium-Ion Battery. *Batteries* 5, 57. doi:10.3390/batteries5030057

Matsuda, Y. (1993). Behavior of Lithium/Electrolyte Interface in Organic Solutions. *J. Power Sourc.* 43, 1–7. doi:10.1016/0378-7753(93)80096-8

Michan, A. L., Parimalam, B. S., Leskes, M., Kerber, R. N., Yoon, T., Grey, C. P., et al. (2016). Fluoroethylene Carbonate and Vinylene Carbonate Reduction: Understanding Lithium-Ion Battery Electrolyte Additives and Solid Electrolyte Interphase Formation. *Chem. Mater.* 28, 8149–8159. doi:10.1021/acs.chemmater.6b02282

Ota, H., Shima, K., Ue, M., and Yamaki, J.-I. (2004). Effect of Vinylene Carbonate as Additive to Electrolyte for Lithium Metal Anode. *Electrochimica Acta* 49, 565–572. doi:10.1016/j.electacta.2003.09.010

Parekh, M. N., Rahn, C. D., and Archer, L. A. (2020). Controlling Dendrite Growth in Lithium Metal Batteries through Forced Advection. *J. Power Sourc.* 452, 227760. doi:10.1016/j.jpowsour.2020.227760

Parekh, M. N., and Rahn, C. D. (2020b). Reducing Dendrite Growth in Lithium Metal Batteries by Creeping Poiseuille and Couette Flows. *J. Electrochem. Soc.* 167 (16), 160525. doi:10.1149/1945-7111/abcf55

Parekh, M., and Rahn, C. (2020a). "Dendrite Suppression and Energy Density in Metal Batteries with Electrolyte Flow through Perforated Electrodes," in . Proceedings of International Mechanical Engineering Congress and Exposition, Virtual, Online, November 16–19, 2020. doi:10.1115/imece2020-23487

Park, J., Jeong, J., Lee, Y., Oh, M., Ryou, M.-H., and Lee, Y. M. (2016). Micro-Patterned Lithium Metal Anodes with Suppressed Dendrite Formation for post Lithium-Ion Batteries. *Adv. Mater. Inter.* 3, 1600140. doi:10.1002/admi.201600140

Pathak, R., Chen, K., Gurung, A., Reza, K. M., Bahrami, B., Pokharel, J., et al. (2020). Fluorinated Hybrid Solid-Electrolyte-Interphase for Dendrite-free Lithium Deposition. *Nat. Commun.* 11, 1–10. doi:10.1038/s41467-019-13774-2

Peled, E. (1979). The Electrochemical Behavior of Alkali and Alkaline Earth Metals in Nonaqueous Battery Systems-The Solid Electrolyte Interphase Model. *J. Electrochem. Soc.* 126, 2047–2051. doi:10.1149/1.2128859

Pinson, M. B., and Bazant, M. Z. (2012). Theory of Sei Formation in Rechargeable Batteries: Capacity Fade, Accelerated Aging and Lifetime Prediction. *J. Electrochem. Soc.* 160, A243–A250. doi:10.1149/2.044302jes

Ploehn, H. J., Ramadass, P., and White, R. E. (2004). Solvent Diffusion Model for Aging of Lithium-Ion Battery Cells. *J. Electrochem. Soc.* 151, A456. doi:10.1149/1.1644601

Ryou, M.-H., Lee, Y. M., Lee, Y., Winter, M., and Bieker, P. (2015). Mechanical Surface Modification of Lithium Metal: towards Improved Li Metal Anode Performance by Directed Li Plating. *Adv. Funct. Mater.* 25, 834–841. doi:10.1002/adfm.201402953

Shi, F., Pei, A., Boyle, D. T., Xie, J., Yu, X., Zhang, X., et al. (2018). Lithium Metal Stripping beneath the Solid Electrolyte Interphase. *Proc. Natl. Acad. Sci.* 115, 8529–8534. doi:10.1073/pnas.1806878115

Single, F., Horstmann, B., and Latz, A. (2017). Revealing Sei Morphology: In-Depth Analysis of a Modeling Approach. *J. Electrochem. Soc.* 164, E3132–E3145. doi:10.1149/2.0121711jes

Single, F., Latz, A., and Horstmann, B. (2018). Identifying the Mechanism of Continued Growth of the Solid-Electrolyte Interphase. arXiv preprint arXiv:1812.03841.

Smith, A. J., Burns, J. C., Xiong, D., and Dahn, J. R. (2011). Interpreting High Precision Coulometry Results on Li-Ion Cells. *J. Electrochem. Soc.* 158, A1136–A1142. doi:10.1149/1.3625232

Tanim, T. R., and Rahn, C. D. (2015). Aging Formula for Lithium Ion Batteries with Solid Electrolyte Interphase Layer Growth. *J. Power Sourc.* 294, 239–247. doi:10.1016/j.jpowsour.2015.06.014

Tikekar, M. D., Archer, L. A., and Koch, D. L. (2014). Stability Analysis of Electrodeposition across a Structured Electrolyte with Immobilized Anions. *J. Electrochem. Soc.* 161, A847–A855. doi:10.1149/2.085405jes

Verma, P., Maire, P., and Novák, P. (2010). A Review of the Features and Analyses of the Solid Electrolyte Interphase in Li-Ion Batteries. *Electrochimica Acta* 55, 6332–6341. doi:10.1016/j.electacta.2010.05.072

Wang, F., Chen, G., Zhang, N., Liu, X., and Ma, R. (2019). Engineering of Carbon and Other Protective Coating Layers for Stabilizing Silicon Anode Materials. *Carbon Energy* 1, 219–245. doi:10.1002/cey2.24

Wang, M., Huai, L., Hu, G., Yang, S., Ren, F., Wang, S., et al. (2018). Effect of Lifsi Concentrations to Form Thickness-And Modulus-Controlled Sei Layers on Lithium Metal Anodes. *The J. Phys. Chem. C* 122, 9825–9834. doi:10.1021/acs.jpcc.8b02314

Wang, S.-H., Yin, Y.-X., Zuo, T.-T., Dong, W., Li, J.-Y., Shi, J.-L., et al. (2017). Stable Li Metal Anodes via Regulating Lithium Plating/Stripping in Vertically Aligned Microchannels. *Adv. Mater.* 29, 1703729. doi:10.1002/adma.201703729

Whittingham, M. S. (2012). History, Evolution, and Future Status of Energy Storage. *Proc. IEEE* 100, 1518–1534. doi:10.1109/jproc.2012.2190170

Zhao, C. Z., Zhao, Q., Liu, X., Zheng, J., Stalin, S., Zhang, Q., et al. (2020). Rechargeable Lithium Metal Batteries with an In-Built Solid-State Polymer Electrolyte and a High Voltage/loading Ni-Rich Layered Cathode. *Adv. Mater.* 32, 1905629. doi:10.1002/adma.201905629

Conflict of Interest: The authors declare that the research was conducted in the absence of any commercial or financial relationships that could be construed as a potential conflict of interest.

Publisher's Note: All claims expressed in this article are solely those of the authors and do not necessarily represent those of their affiliated organizations, or those of the publisher, the editors and the reviewers. Any product that may be evaluated in this article, or claim that may be made by its manufacturer, is not guaranteed or endorsed by the publisher.